

## Estimates of mantle relevant Clapeyron slopes in the MgSiO<sub>3</sub> system from high-pressure spectroscopic data

A. CHOPELAS\*

Max Planck Institut für Chemie, Postfach 3060, 55020 Mainz, Germany

### ABSTRACT

The phase diagram for MgSiO<sub>3</sub> was estimated using the entropy, enthalpy, thermal expansivity, and volumes of all the phases. Entropy at the various *P-T* conditions in the phase diagram was estimated using statistical thermodynamics and spectroscopic data at ambient and high pressures for each of the phases. Nearly complete 1 atm polarized Raman spectra of end-member MgSiO<sub>3</sub>, orthoenstatite and new high-pressure Raman data on orthoenstatite (*Pbca*) to 24.5 GPa and majorite to 33.6 GPa are presented. Both of these minerals exhibit profound changes in their spectra as pressure is increased and the pressure dependence of the Raman modes changes substantially at 5 GPa for orthoenstatite and 26 GPa for majorite. These, like MgSiO<sub>3</sub>, perovskite, appear to change symmetry even at room temperature. The slopes for the following transitions are reported: clinoenstatite (*C2/c*) to majorite, –12 bar/K; majorite to ilmenite, 46 bar/K; ilmenite to perovskite, –46 bar/K, majorite to perovskite, 26 bar/K. A volume change of 0.6 cm<sup>3</sup>/mol for the orthopyroxene to high-pressure clinopyroxene transition was estimated using the previously measured phase boundary and the present entropy data. Clapeyron slopes are overestimated by 20 to 100% if the pressure dependence of  $\Delta S$  across the transitions at various *P-T* conditions is not included in the thermodynamic calculations.

### INTRODUCTION

Thermodynamic parameters have been used to check the consistency of phase equilibrium data as well as to extrapolate the phase boundaries beyond the usually limited *P-T* space of the experiments (for example, Akaogi et al. 1989; Chopelas et al. 1994a). The ability to accurately predict phase boundaries among candidate mantle minerals aids in modeling of mantle compositions and temperatures at the seismic discontinuities and in modeling the topography of phase boundaries due to lateral temperature variations. Very often, large uncertainties in the slopes of phase boundaries exist due to the limited number of data taken over a too narrow *P-T* range in phase equilibrium experiments. The required long extrapolations of these phase boundaries render them unsuitable for the purpose of modeling the Earth's mantle. Estimates of the phase boundaries using the thermodynamic parameters complement phase boundary measurements at high *P* and *T*.

The required parameters for estimating phase boundaries are change in enthalpy,  $\Delta H$ , change in entropy,  $\Delta S$ , heat capacity,  $C_p$ , and change of volume  $\Delta V$  across the phase transition. Enthalpies are measured by calorimetry (for example, Akaogi and Ito 1993b; Akaogi et al. 1989) and entropies and heat capacities are derived from spectroscopic measurements using statistical thermodynamics. Volumes are derived from compression measurements at

room temperature and thermal expansivity systematics (Chopelas and Boehler 1992b). This study presents new spectroscopic data for orthoenstatite and majorite, and uses these and previous data for perovskite (Chopelas 1996), ilmenite (Hofmeister and Ito 1992; Reynard and Rubie 1996), and clinoenstatite (Chopelas and Boehler 1992a) in the MgSiO<sub>3</sub> system to estimate entropy and heat capacities. The MgSiO<sub>3</sub> phase diagram is then predicted using these new data with the previous calorimetric and volumetric data.

### EXPERIMENTAL METHODS

For all Raman measurements on MgSiO<sub>3</sub> polymorphs, synthetic end-member orthoenstatite (Smithsonian no. 137311) was heated in the diamond cell to the appropriate temperature at various pressures to produce clinoenstatite (17 GPa), majorite (18 GPa), ilmenite (18 GPa), and perovskite (21 GPa).

Polarized Raman spectra of orthoenstatite were collected at one atm from approximately 1 mm single crystals oriented using its natural crystal faces. Typical laser powers at the sample were about 10 to 20 mW. For all measurements at high pressures, a chip from the same orthoenstatite was loaded in a diamond cell where the diamonds had 250  $\mu\text{m}$  diameter culets. The sample and micrometer-sized ruby chips were placed in the 100  $\mu\text{m}$  diameter gasket chamber, which was then filled with high purity dry argon in a single-cylinder, 0.3 GPa gas pressure vessel using a membrane compressor. To obtain the

\* E-mail: chopelas@mpch-mainz.mpg.de

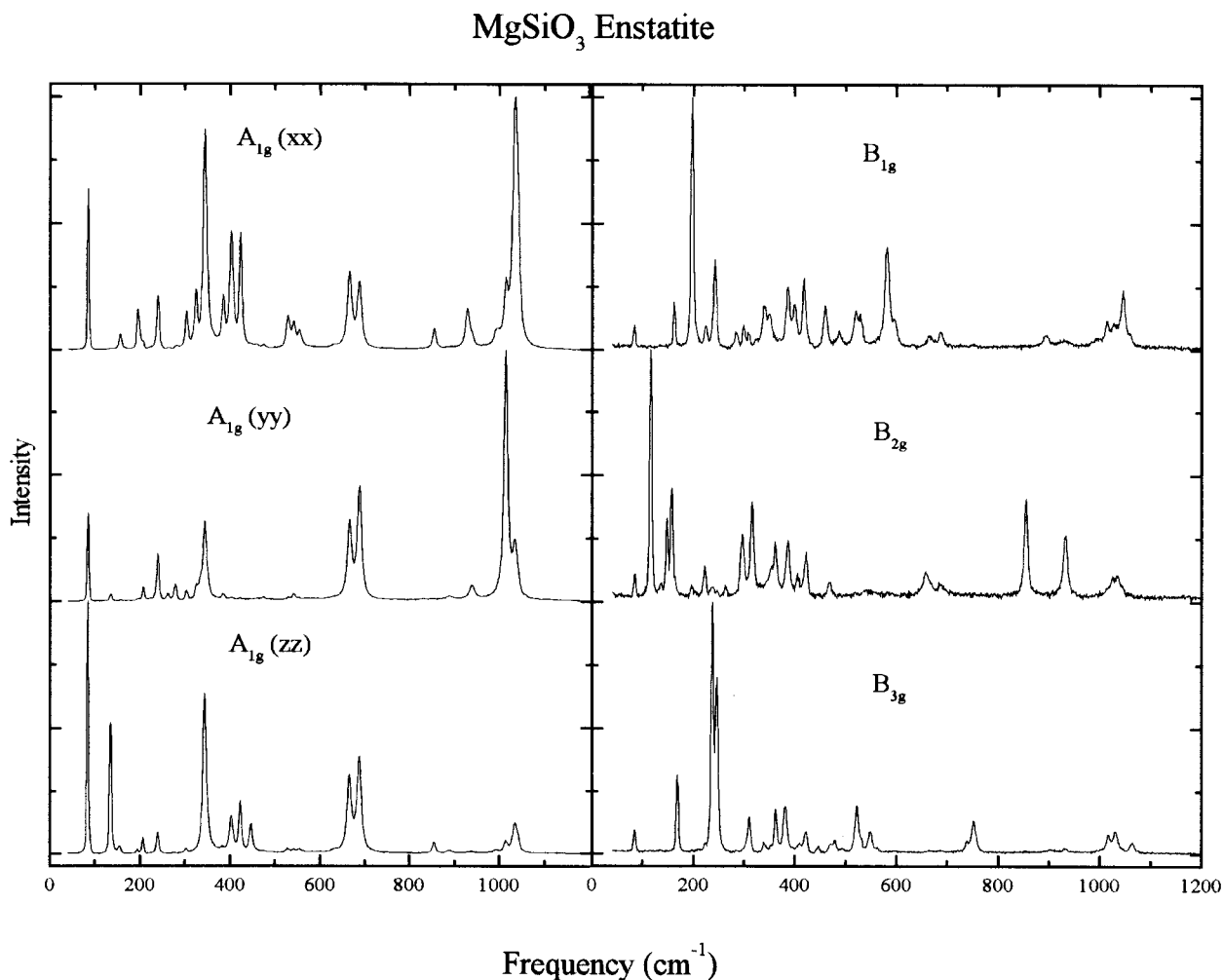


**FIGURE 1.** Polarized Raman spectrum of  $\text{MgSiO}_3$  orthoenstatite (*Pbca* space group). Symmetries and polarization of incoming and outgoing laser beam relative to the crystal axes are indicated. The Raman shifts are listed in Table 1. These are raw spectra; no baseline corrections were needed.

different polymorphs, the orthoenstatite sample was heated with a  $\text{CO}_2$  laser (Boehler and Chopelas 1992) at the pressures named above. Further measurements at various pressures were then undertaken, usually first by compression in small pressure steps, then by decompression. For the orthoenstatite pressure run, the initial pressure was 3.5 GPa and spectra were taken at several intermittent pressures up to the final pressure of 24.5 GPa, after which spectra were taken at decreasing pressures down to atmospheric pressure. Pressure cycles for the other polymorphs were as follows: clinoenstatite, decreased pressure from 17 GPa to 1 atm; majorite, increased pressure from 18 GPa to 34 GPa then reduced to 11 GPa; ilmenite, 19.6 GPa; perovskite, in several runs increased from 21 GPa to 45 GPa then decreased to 17 GPa and also synthesized at 65 GPa then decreased to 40 GPa after which the spectrum disappeared (Chopelas 1996). The Raman spectra were excited with either the 488.0 nm or the 457.9 nm line of a Spectra Physics 2025-5 argon ion laser. The

laser light entered the diamond cell at an incident angle of  $25^\circ$  and was focused to a  $10\ \mu\text{m}$  spot on the sample. Typical laser powers at the sample ranged from 10 to 20 mW, too low to cause heating. The degree of heating was monitored by (1) checking for peak shifting while changing the laser power and (2) by examining the anti-Stokes/Stokes intensity ratios. The Raman signal entered the monochromator through a pinhole to minimize interference from the diamond fluorescence. Raman spectra were analyzed using an ISA U1000 double monochromator with a photon counting system. The spectra were sampled at  $0.8\ \text{cm}^{-1}$  intervals. All spectra were collected at  $294 \pm 1\ \text{K}$ .

#### THERMODYNAMIC CALCULATIONS

Setting the Gibbs free energy,  $\Delta G$ , to zero in the following equation allows the calculation of the phase boundaries:

**TABLE 1.** Frequencies in inverse centimeters of polarized Raman spectrum of MgSiO<sub>3</sub> orthoenstatite

A <sub>g</sub>	B <sub>1g</sub>	B <sub>2g</sub>	B <sub>3g</sub>
83	—	115	—
134	161	135	133
153	197	147	168
193	223	156	197
206	241	197	208
239	283	234	237
261	297	263	245
279	308	296	284
302	339	315	309
323	349	353	338
334	385	360	353
343	398	386	361
384	417	403	380
402	458	421	394?
422	486	466	408
446	519	487	421
457	527	516	445
473	580	541	468
528	595	581	478
540	630	—	500
553	—	—	521
630	663	656	548
665	686?	685?	738
687	749	752	751
853	892	854	—
886	897	—	903
927	928	931	931
937	1027	1024	1016
1014	1044	1044	1030
1034	1057	—	1063

Notes: Peaks marked “?” are uncertain in this polarization.

$$\Delta G_{P,T}^0 = 0 = \Delta H_{P,T}^0 - T\Delta S_{P,T}^0 + \int_0^P \Delta V \cdot dP \quad (1)$$

where  $\Delta H$  the enthalpy of transition,  $T$  is the temperature,  $\Delta V$  the change in volume across the phase boundary, and  $P$  the pressure. The enthalpy is measured by calorimetry and the volumes are estimated from elastic constants, an equation-of-state, and the thermal expansivity. The entropy  $\Delta S$  in most previous phase boundary calculations was estimated by selecting one point along a measured phase boundary, solving for entropy using Equation 1 and then calculating the remaining phase boundary using this value. If the point chosen does not lie on the true phase boundary, meaningless results are obtained.

Statistical thermodynamics and data from vibrational spectroscopy allow entropy to be obtained independently. First, with a good vibrational model density of states for the mineral, the constant volume heat capacity  $C_V$  can be estimated from

$$C_V = 3Nk \int_0^\infty \frac{e^x}{(e^x - 1)^2} x^2 g(\nu) d\nu \quad (2)$$

where  $N$  is the number of atoms in the unit cell,  $k$  is Boltzmann's constant,  $\nu$  is the frequency of vibration,  $x$  is  $h\nu/kT$ ,  $h$  is Planck's constant, and  $g(\nu)$  is the density of states. Then  $C_V$  can be converted to the constant pressure heat capacity  $C_P$  using

$$C_P = C_V + TV\alpha^2 K_T \quad (3)$$

**TABLE 2.** Vibrational models for MgSiO<sub>3</sub> minerals

Lower limit	Upper limit	Number of modes	$\gamma_i$
<b>Pbca Orthoenstatite</b>			
0	65	1	0.2
0	67	1	0.3
0	110	1	1.23
83	90	3	2.32
110	120	3	3.26
120	140	5	3.3
140	168	10	1.46
168	223	12	1.75
223	245	12	1.23
245	323	28	1.25
323	350	12	1.93
350	362	12	1.1
380	390	8	1.1
398	447	32	0.7
516	553	20	0.7
580	630	16	0.6
656	752	16	0.63
853	903	12	0.36
886	937	16	0.55
1014	1035	20	0.62
<b>C2/c Clinoenstatite</b>			
0	95	1	0.80
0	104	1	0.80
0	172	1	2.4
120	155	2	1.10
165	484	6	1.7
216	280	2	0.90
229	416	11	1.4
380	577	20	0.64
680	682	2	0.57
714	716	2	0.46
829	831	5	0.43
1005	1007	4	0.54
1023	1026	3	0.62
<b>I4/a Majorite</b>			
0	70	1	0.75
0	70	1	0.75
0	140	1	1.3
136	400	60	1.42
350	400	36	1.305
195	400	33	1.305
458	723	60	0.86
803	1081	48	0.86
<b>R<math>\bar{3}</math> Ilmenite</b>			
0	168.7	1	0.75
0	184.5	1	0.75
0	301.3	1	1.3
287	337	2	1.6
337	595	13	1.35
595	700	10	1.1
735	799	2	1.1
<b>Pbmn Perovskite</b>			
0	130	1	0.85
0	150	1	0.85
0	223	1	2.5
240	335	12	1.8
335	440	12	1.1
440	540	15	0.95
590	680	9	0.75
700	780	7	0.75
890	891	2	0.75

Notes: The first three modes in each of the models represent the acoustic modes. The remainder are optic mode continua. Einstein oscillators are simply assigned very narrow frequency ranges that facilitated the calculations at high pressures. The mode Grüneisen parameters,  $\gamma_i$ , are used to obtain the pressure shifts of the frequency ranges using the bulk moduli listed in Table 6.

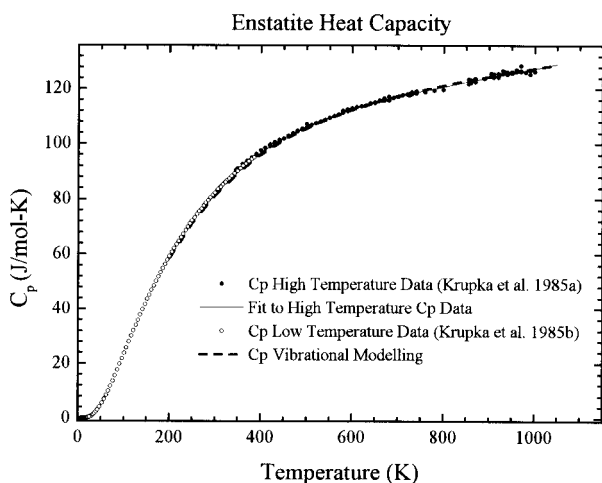


**FIGURE 2.** Comparison of the spectroscopically derived constant pressure heat capacity  $C_p$  and that measured by calorimetry (Krupka et al. 1985a; Krupka et al. 1985b). The spectroscopic value, dashed line, falls nearly on all the data in the figure.

where  $\alpha$  is the thermal expansivity and  $K_T$  is the isothermal bulk modulus. To obtain entropy, Equation 4 is integrated over temperature:

$$dS = \int_0^{T_1} \frac{C_p}{T} dT \quad (4)$$

where  $T_1$  is the temperature of interest.

However, in the earlier papers using this method, (e.g., Akaogi et al. 1989),  $\Delta S$  was held constant under different pressure and temperature conditions although  $\Delta H$  and  $\Delta V$  were varied for  $P$  and  $T$ . Variations of  $\Delta H$  with temperature were estimated using the heat capacity obtained from Equation 3 in

$$\Delta H^0(T) = \Delta H^0(T_0) + \int_{T_0}^T \Delta C_p \cdot dT \quad (5)$$

In this study, changes in volume are estimated by first using the bulk modulus and its pressure dependence in the third-order finite strain equation-of-state (Birch 1978) to compress the volume. Then the volumes are corrected for temperature with the 1 atm thermal expansivity, which is adjusted for pressure using thermal expansion systematics (Chopelas and Boehler 1992b). This method circumvents the need to compress the materials at high temperatures where the bulk moduli are poorly known. Thermal expansivity was checked for internal consistency using the Maxwell relation,  $(\partial S/\partial P)_T = -(\partial V/\partial T)_P$ , where the pressure dependence of the entropy is derived from the spectroscopic data, as described previously (Chopelas 1996).

### ORTHOENSTATITE

Orthoenstatite belongs to the  $Pbca$  space group ( $D_{2h}$ ) with eight formula units ( $Mg_2Si_2O_6$ ) per unit cell. The 80 atoms per unit cell require 240 vibrations ( $3n$ , where  $n$  is

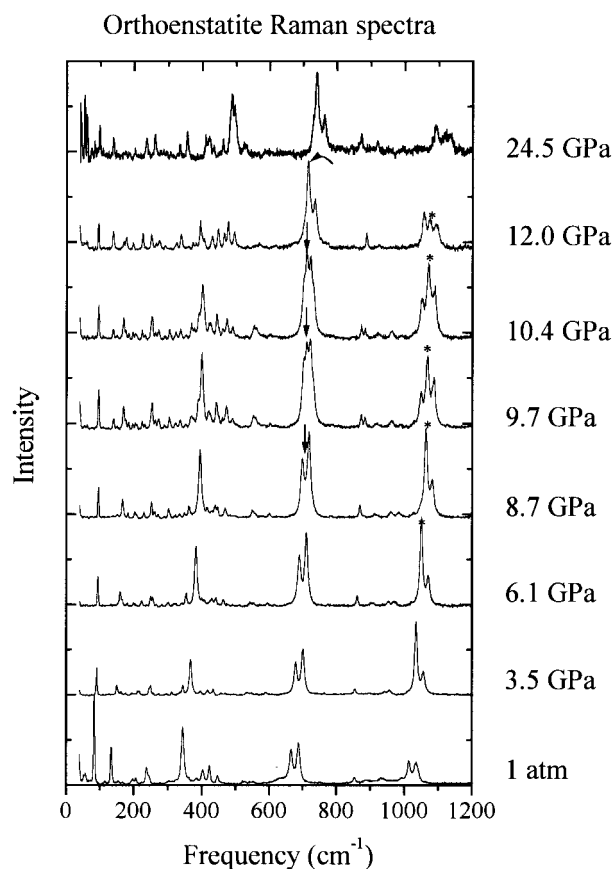


**FIGURE 3.** Spectrum of orthoenstatite at various pressures. The intensity of the peaks at 1 atm varies slightly from those between 3.5 and 8.7 GPa because the crystals were at slightly different orientations. However, all spectra within the diamond cell were taken at nearly the same orientation. The arrow at 8.7 GPa indicates where the new peak appears at higher pressures and the asterisk at 6.1 GPa indicates a prominent peak that gradually disappears until it is no longer visible above 12 GPa. At 12 GPa the transformation process is nearly complete.

number of atoms per unit cell) at any one point in the Brillouin zone. All atoms in the formula unit are unique and of  $C_1$  symmetry: the vibrations are distributed evenly among all the symmetry species. The irreducible representation for orthoenstatite is:

$$\Gamma = 30A_{1g}(R) + 30B_{1g}(R) + 30B_{2g}(R) + 30B_{3g}(R) \\ + 30A_{1u} + 30B_{1u}(IR) + 30B_{2u}(IR) + 30B_{3u}(IR)$$

where R and IR denote Raman or infrared activity, respectively, of the various vibrational symmetries. Thus, there are 30 vibrations in each of the four Raman symmetries for a total of 120 Raman active modes. The polarized single crystal Raman spectra of the orthoenstatite sample (Fig. 1) reveals 112 of these modes (Table 1) on a very low background fluorescence. The mode at 83  $cm^{-1}$  is not easily obtainable by most spectrometers (especially those with multichannel devices requiring inter-

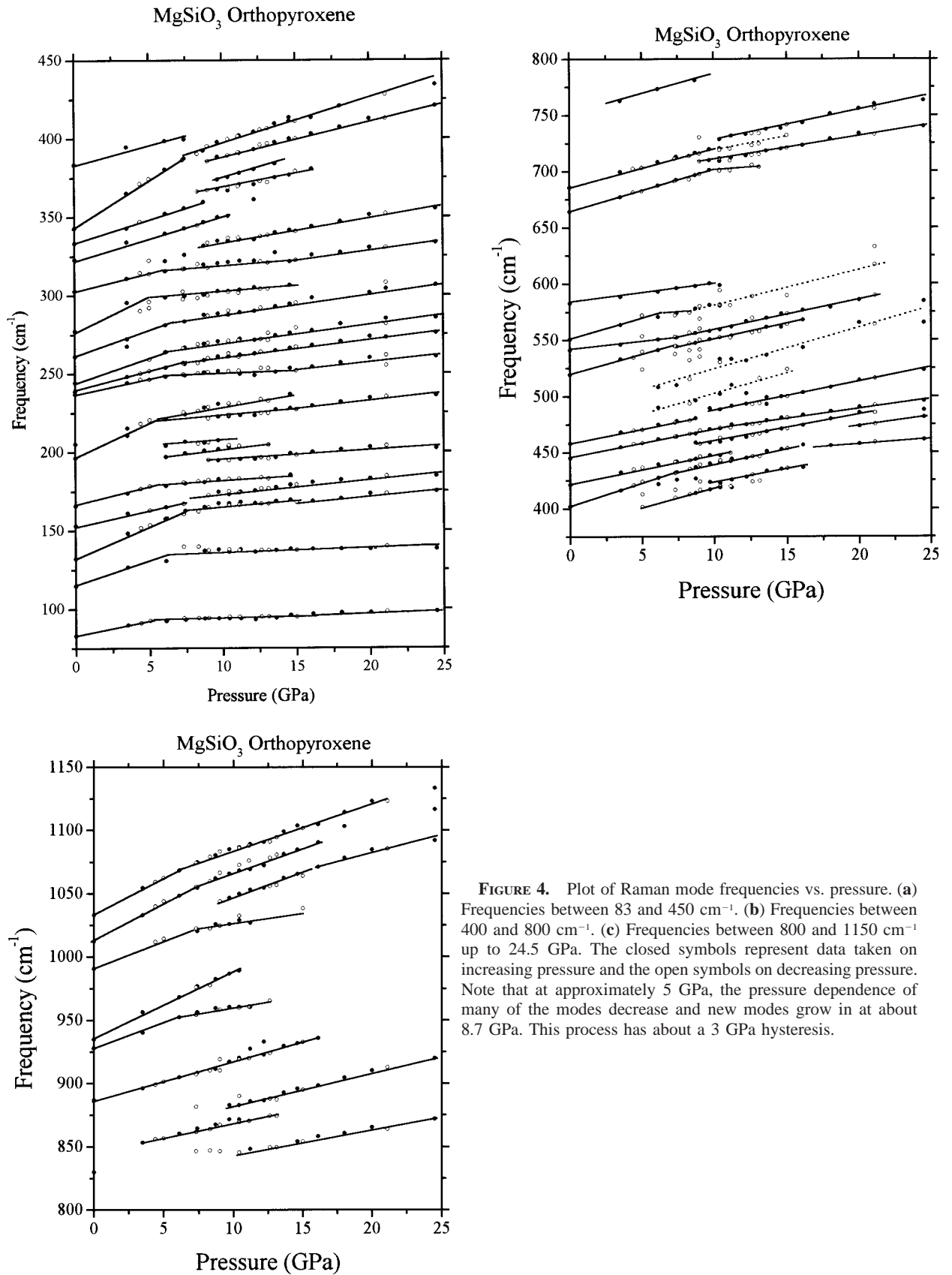


**TABLE 3.** Slopes in cm<sup>-1</sup>/GPa and mode Grüneisen parameters of the vibrational modes in MgSiO<sub>3</sub> orthopyroxene

Frequency (cm <sup>-1</sup> )	1 atm		Above 5 GPa	
	Slope	γ	$\nu_0$ intercept	Slope
83	1.8	2.32	87	0.45
115	3.5	2.36	135	0.22
134	4.16	3.33	162	0.44
153	2.1	1.46	169	0.55
166	2.2	1.52	185	0.8
197	3.4	2.11	214	1.0
237	3	1.35	237	1.2
239	1.4	0.63	249	1.15
245	3.3	1.44	278	1.05
261	3.6	1.48	310	1.1
302	2.6	0.921	320	1.5
343	6.2	1.93	362	2.5
402	4.3	1.14		
422	3	0.76		
446	2.6	0.26	441	0.8
457	3	0.30	465	2.65
487	3.8	0.83		
519	5.2	0.87		
540	2.5	0.50		
553	3.1	0.60		
580	4.2	0.44		
665	4	0.65	698	2.75
687	3.7	0.58	717	2.05
886	3	0.36	857	2.55
927	4	0.46		
937	6	0.67		
1014	6.2	0.65	1042	2.1
1034	5.9	0.61	1055	3.3

mediate slits and exit slits on the monochromator to be open 12 to 25 mm, which does not allow simple measurement of vibrational modes near the excitation laser line). This mode is a Raman fundamental because its intensity changes as the crystal is rotated, and its frequency shifts as pressure is applied to the sample (see below). A mode very near this frequency was also seen in the Fe-bearing orthoenstatite (Chopelas, unpublished data) and β-Mg<sub>2</sub>SiO<sub>4</sub> (Chopelas 1991), a material also containing Si-O-Si linkages. In A<sub>1g</sub>, all 30 of the predicted modes were found, and in each of the B symmetries, nearly all of the modes were found. The modes were distributed similarly in each of the symmetries, suggesting that this is also the case for the u symmetries that are either spectroscopically inactive or infrared active.

Because so many Raman active modes exist, an accurate frequency distribution can be simply obtained by constructing a histogram of the modes vs. frequency. The model need only be altered to consider such things as the acoustic modes, the stretching vibrations that separate out from the main vibrational continuum, and the modes that shift quite differently with pressure than the others (i.e., those containing predominately Mg translational character). This information can be easily obtained from symmetry considerations. From factor group analysis (Fateley et al. 1971), 48 vibrations are attributed to the translation of Mg cations, 6 in each symmetry. These are grouped in with SiO<sub>4</sub> translations, rotations, and internal bending modes. They can be determined by either cation substi-

**TABLE 4.** MgSiO<sub>3</sub> clinopyroxene (C2/c space group) table of Raman frequencies and their pressure dependencies

$\nu_0^*$ in cm <sup>-1</sup>	Slope	$1/\nu_0(\partial\nu/\partial P)_{T,P=0} \times 10^4$	γ†
172.5	1.0	0.58	0.71
216.5	1.71	0.79	0.99
229	1.63	0.71	0.99
253	0.87	0.34	0.43
315	2.13	0.68	0.83
320	3.90	1.22	1.5
366	3.31	0.90	1.1
378	5.57	1.5	1.8
451.5	2.84	0.63	0.78
528	3.44	0.65	0.80
529	1.0	0.19	0.23
681	3.19	0.47	0.58
751	2.91	0.39	0.48
829	2.94	0.35	0.43
914	2.27	0.25	0.30
1006	4.50	0.45	0.54
1024	5.20	0.51	0.62

Notes: Slope units are cm<sup>-1</sup>/GPa.

\* Frequencies were extrapolated to room pressure.

† The bulk modulus = 123 GPa (Angel et al. 1992). This value cancels out in the calculation of the thermodynamic parameters.

tution or measuring their shift with pressure, which will be greater because the Mg cations are in a more compressible part of the pyroxene structure. Two Si-O-Si bonds and four Si-O bonds are present for each Si<sub>2</sub>O<sub>6</sub> unit in the silicate chain. The Si-O-Si bonds give rise to two symmetric and two antisymmetric vibrations, and the four Si-O bonds give rise to four vibrations, a total of eight per Si<sub>2</sub>O<sub>6</sub> unit. Because eight Si<sub>2</sub>O<sub>6</sub> units exist per unit cell, there are a total of 64 Si-O stretching vibrations per unit cell, 16 symmetric and 16 antisymmetric of the bridging bonds and 32 stretches of the non-bridging bonds. The nonbridging bonds vibrate at higher frequencies than the bridging bonds. The resulting frequency distribution or density of states based on this information is listed in Table 2 (top) and yields a C<sub>p</sub> in exact agreement with available calorimetric data (Krupta et al. 1985a, Krupta et al. 1985b) (Fig. 2).

## HIGH-PRESSURE RESULTS

The pressure shift of the thermodynamic parameters can be calculated using the high-pressure Raman results, shown in Figure 3. The frequencies are plotted vs. pressure in Figure 4. In Figure 4, at 5 GPa nearly all modes show a change in slope, indicating that the compressional mechanism has changed. Above this pressure, at about 8.7 GPa, the prominent orthoenstatite peaks weaken in intensity, while new peaks start to grow in. At 12 GPa, the orthoenstatite peaks are gone, and the new spectrum still appears to be that of a chain silicate but of a different structure. At the highest pressures of this study, the final spectrum appears very similar to that of diopside and the C2/c clinopyroxene previously reported (Chopelas and Boehler 1992a). All these effects are reversible with a slight hysteresis. At higher temperatures, the stable phase

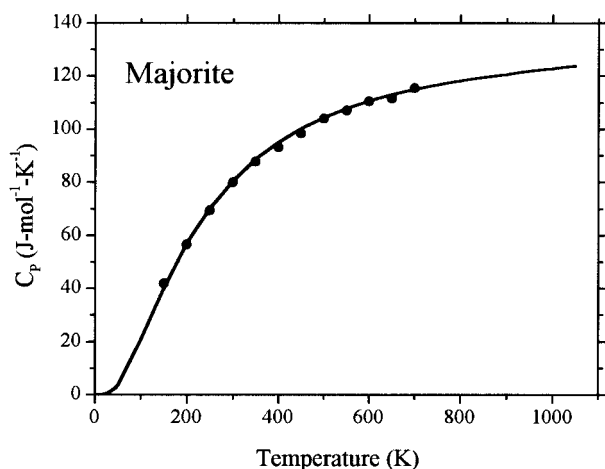


FIGURE 5. Comparison of the spectroscopically derived heat capacity (solid line) for MgSiO<sub>3</sub> majorite to that measured by calorimetry (points) by Yusa et al. (1993).

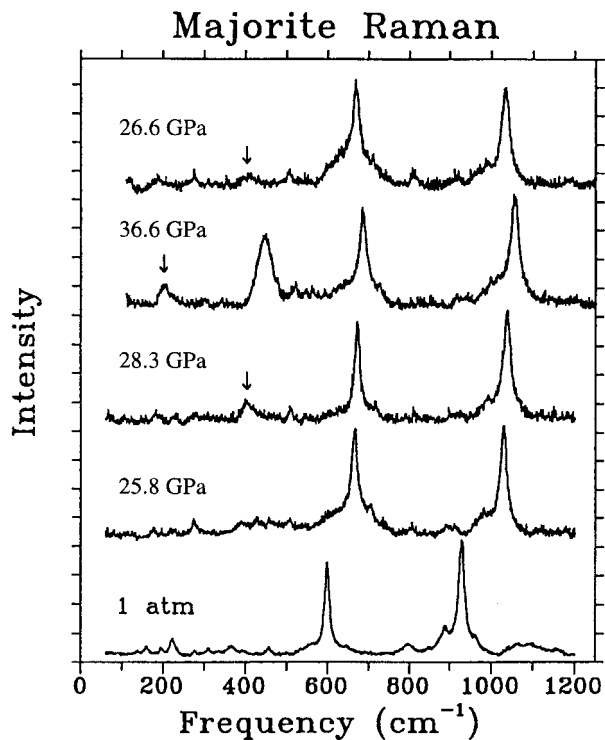


FIGURE 6. Plot of MgSiO<sub>3</sub> majorite Raman spectrum at five different pressures. At 28.3 GPa, a new mode begins to grow in, indicated by the arrow. At the highest pressure, 33.6 GPa, this mode becomes one of the most prominent in the spectrum. A second relatively strong mode has grown in around 200 cm<sup>-1</sup>, also indicated by an arrow, and many of the minor modes between 200 and 600 cm<sup>-1</sup> have disappeared. As the pressure is reduced to 26.6 GPa (top spectrum in the figure), these two new prominent peaks disappear. The spectrum at 33.6 GPa strongly resembles that of cubic garnet.

TABLE 5. Pressure dependence of the majorite Raman modes

Frequency (cm <sup>-1</sup> )	Slope (cm <sup>-1</sup> /GPa)	$\gamma_i$	Line above 26.6 GPa	Frequency (cm <sup>-1</sup> )†	Slope (cm <sup>-1</sup> /GPa)
136	1.61	1.77		196	0.92
195*	1.2	0.90		200	0.72
			190 + 3.45 P	222	1.98
				234	1.25
				255	1.9
277*	1.7	0.97		273	1.69
311*	1.9	0.92		308	1.73
334	2.53	1.14	276 + 5.06 P	332	2.17
				355	2.05
367*	2.32	0.95		365	2.6
398*	2.34	0.54		397	2.7
				428	2.1
				456	1.62
458	1.83	0.60		494	1.44
				516	1.61
				533	2.11
				554	2.5
602	2.51	0.625		599	2.49
648	2.34	0.542		647	2.31
690	4.2	0.90			
802	3.39	0.63	936 + 1.86 P	800	3.8
				853	3.9
889	3.93	0.66		885	3.8
931	4.2	0.67		930	3.7
				964	3.9
				1065	4.1

\* Data taken from 17 to 24 GPa and at ambient conditions, see Fig. 7.

† Data of Rauch et al. (1996) to 21 GPa, no data plot was published so it is difficult to assess sources of the minor differences.

is high-pressure clinoenstatite, meaning that the phenomenon observed here is the thermally hindered transformation to this structure. In any case, calculation of the thermodynamic parameters based on the model in Table 3, first section, are not extended beyond 5 GPa. The stable phase above this pressure is actually the *C2/c* structure.

#### CLINOENSTATITE

The next high-pressure polymorph of orthoenstatite is the unquenchable high-pressure clinoenstatite, space group *C2/c*, the same structure as diopside. If the pressure on this phase drops below about 5.1 GPa, it reverts to low-pressure clinoenstatite, space group *P2<sub>1</sub>/c* (Angel et al. 1992). The irreducible representation for high-pressure clinoenstatite is  $14 A_g(R) + 16 B_g(R) + 13 A_u(IR) + 15 B_u(IR)$ . The spectrum of this phase is nearly identical to diopside at the same pressures (Chopelas and Boehler 1992a) except that a few of the modes are substantially increased in frequency due to the substitution by the much lighter Mg for the Ca. The density of states for the high clinoenstatite phase in Table 2 (second section) was based on that for diopside, which used the nearly complete spectral information (Etchepare 1970; Chopelas, unpublished work). Only 6 of the 30 Raman fundamentals,  $2 A_g$  and  $4 B_g$ , are related to the Mg cations, so very few of the 60 vibrations will be affected by the substitution of the Ca by the Mg in the high clinoenstatite phase.

The model for diopside was tested to see if it yielded a heat capacity that agreed with calorimetric measure-

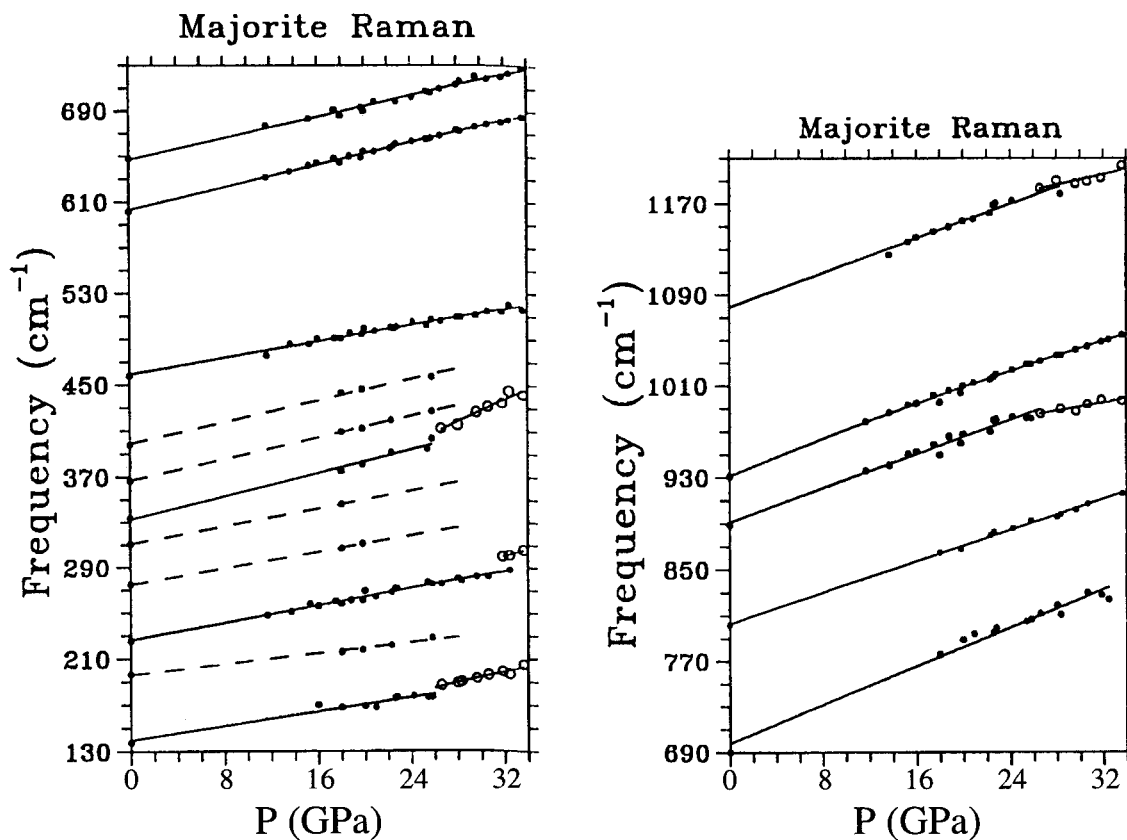


**FIGURE 7.** Plot of the majorite Raman mode frequencies vs. pressure (a) between 130 and 730  $\text{cm}^{-1}$  and (b) between 690 and 1210  $\text{cm}^{-1}$  from 1 atm to 33.6 GPa. The dashed lines represent weak modes that disappeared above 26 GPa and did not reappear as the pressure was reduced. However, the few data points that do exist for these modes extrapolated to the values measured at 1 atm on a sample produced in a large volume press (measured in our laboratory). The hollow points are the new modes that grew in above 26 GPa and disappeared again as the pressure was decreased below this point.

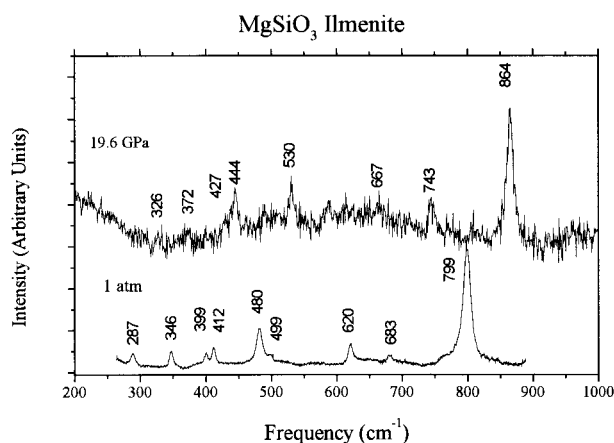


**FIGURE 8.** Spectrum of  $\text{MgSiO}_3$  ilmenite produced in the  $\text{CO}_2$  laser heated diamond cell at 19.6 GPa compared to that taken at room conditions. These data agree well with previous Raman high-pressure data (Reynard and Rubie 1996).

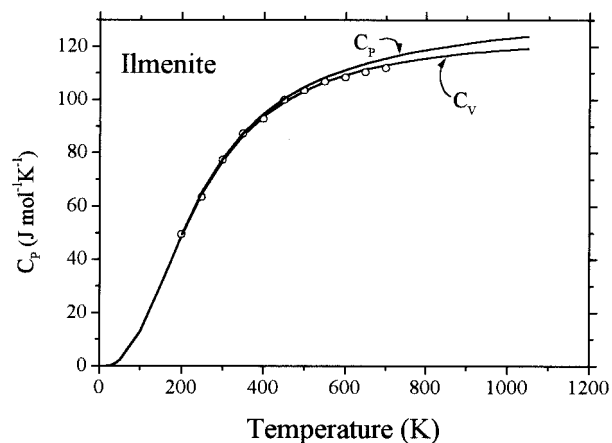


**FIGURE 9.** Comparison of the spectroscopically derived heat capacities of  $\text{MgSiO}_3$  ilmenite (solid lines, one for  $C_v$  and one for  $C_p$ , as indicated on Fig. 9) to that measured by calorimetry (points) (Ashida et al. 1988).

**TABLE 6.** Thermal properties of the MgSiO<sub>3</sub> phases

	Ortho- ensta- tite	Clino- ensta- tite	Perov- skite	Majorite	Ilmenite
$K_{0T}$ (GPa)	96 <sup>a</sup>	123.0 <sup>a</sup>	263 <sup>e</sup>	160 <sup>a</sup>	210 <sup>h</sup>
$K'_{0T}$	14.9 <sup>a</sup>	5.6 <sup>a</sup>	4 <sup>f</sup>	4.5 <sup>d</sup>	4.0 <sup>f</sup>
$\alpha_{298}$ (10 <sup>6</sup> /K)	43 <sup>b</sup>	29 <sup>c</sup>	18 <sup>b</sup>	20 <sup>b</sup>	16.7 <sup>b</sup>
$V_{298}^0$ (cm <sup>3</sup> /mol)	31.32	30.43 <sup>d</sup>	24.51	28.58	26.35

*Notes:* a. Hugh-Jones and Angel (1994); Note for orthoenstatite: Flesch et al. (1998) report polycrystalline ultrasonic values of  $K = 104$  GPa,  $K'$  of 10.9, and  $K''$  of  $-1.6$  GPa<sup>-1</sup> up to 10 GPa pressure. I chose the single crystal values, but both yield nearly the same volumes in the equation of state for the pressure range of interest. b. Calculated from the Maxwell relation and  $(\partial S/\partial P)_T$  in this study, see Chopelas (1996). c. Assumed close to forsterite. d. Angel et al. (1992). e. Weidner et al. (1993). f. Assumed. g. Yagi et al. (1992). h. Weidner and Ito (1985).

ments (Krupka et al. 1985a, 1985b), then the modes affected by the cation substitution were accounted for. The model density of states for high clinoenstatite could not be checked against any calorimetry because it is not a quenchable phase. However, the present calculated entropy change ( $-2.8$  J/mol·K) for the ortho to clinoenstatite transition at 5 GPa yielded a very reasonable  $-0.6$  cm<sup>3</sup>/mol volume change when the measured Clapeyron slope of 31 bar/K (Pacalo and Gasparik 1990) was used to calculate this volume change. This volume change is consistent with that inferred from single crystal compression data on clinoenstatite, and the entropy change is in line with that obtained by thermodynamic modeling of the enstatite-diopside join at low pressure (Angel et al. 1992).

Details of the high-pressure Raman spectra and the pressure dependencies of the Raman modes were published by Chopelas and Boehler (1992a). The frequencies and pressure dependencies are listed in Table 4. To facilitate comparisons among the various minerals in this study, mode Grüneisen parameters were calculated using a bulk modulus of 123 GPa (Hugh-Jones and Angel 1994). In the thermodynamic calculations, the bulk modulus was canceled but was needed for estimating volumes at high pressures.

### MAJORITE

Garnets in the tetragonal distortion, space group  $I4_1/a$ , have many more active infrared and Raman modes than garnets in the cubic structure. For tetragonal garnets, the irreducible representation is  $25A_g(R) + 27B_g(R) + 28E_g(R) + 32A_u(IR) + 31B_u + 33E_u(IR)$ . Thus, nearly all of the vibrational modes of this garnet should be seen by infrared and Raman spectroscopy. However, no single-crystal spectra exist for tetragonal majorite garnet, but many modes have been measured by both infrared and Raman spectroscopy (McMillan et al. 1989). A vibrational model for majorite was adapted from the model for the cubic garnet pyrope (Hofmeister and Chopelas 1991a) and considering (1) that sixfold-coordinated aluminum is replaced with sixfold-coordinated Si and Mg, and (2) the mode distribution found in the 1 atm data. Because the spectroscopic data is fairly incomplete, fewer ranges were

**TABLE 7.** Enthalpy changes for phase transitions in MgSiO<sub>3</sub> in kJ/mol

Cen to Maj	33.0 ± 3.0*
Maj to Ilm	25.0 ± 5.3†
Maj to Pv	79.7 ± 5.2†
Ilm to Pv	54.7 ± 6.6†

\* This work.  
† From Yusa et al. (1993).

used (Table 2, third section). The resulting heat capacity at one atmosphere matched that of the available calorimetric data (Yusa et al. 1993) very well (Fig. 5).

### HIGH-PRESSURE RESULTS

Calculating thermodynamic properties of majorite garnet to mantle conditions requires high-pressure spectroscopic data. Raman spectra were taken at 1 atm and from 11 to 33.6 GPa, which is well above the stability pressure of this phase. Frequency increased linearly with pressure from 1 atm to about 26.6 GPa. Above 28.3 GPa, two new peaks begin to appear in the spectrum and several of the minor peaks disappear (Fig. 6). At higher pressures, the spectrum of majorite resembled the spectrum of cubic garnets (Hofmeister and Chopelas 1991b) because of further intensity changes. Upon decompression, the new prominent peaks disappeared below  $P = 26.6$  GPa (Fig. 6). The pressure dependence of the modes are listed in Table 5, including the peaks that appeared above 26.6 GPa (Fig. 7). These compare well with lower pressure results by other investigators (Rauch et al. 1996). The density of states used in Equation 2 was shifted according to the pressure dependencies of the Raman modes below 26.6 GPa.

### ILMENITE

Ilmenite, space group  $R\bar{3}$  with two formula units in the primitive cell, yields 30 normal modes of vibration at any one point in the Brillouin zone distributed at the zone center as follows:  $5A_g(R) + 5E_g(R) + 5A_u(IR) + 5E_u(IR)$ .

Raman and infrared data from the literature and high-pressure data from this study and the literature (Hofmeister and Ito 1992; Reynard and Rubie 1996) were used to establish a simple model of the vibrational spectrum. Previous work from this laboratory (Boehler and Chopelas 1992) extended the pressure data to nearly 20 GPa and the values for the mode frequencies were nearly those that lie on the extrapolated lines from other work (Reynard and Rubie 1996). Thus, no obvious changes in the spectrum (Fig. 8) or the pressure dependencies of the modes are seen here. The model density of states (Table 2, fourth section) reproduced the heat capacity values from calorimetry (Ashida et al. 1988), showing deviations of the calculated values by only 3% from the experimental values (Fig. 9). A similar discrepancy was seen between calculations based on IR data (Hofmeister and Ito 1992) and attributed to experimental uncertainty as this calorimetric study also yielded  $C_p$  values for pyroxene

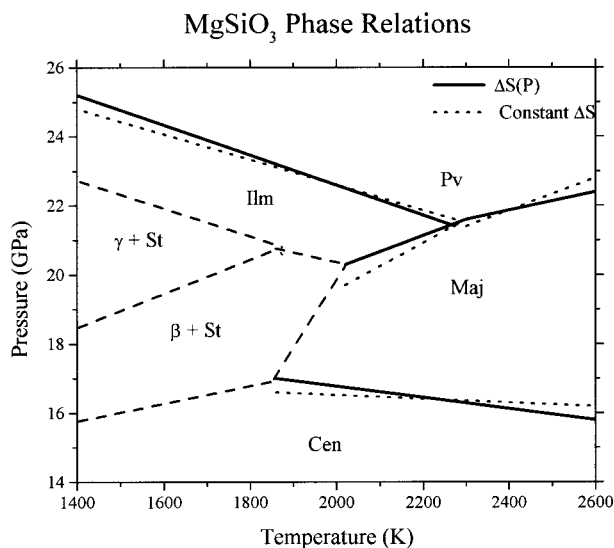


**FIGURE 10.**  $\text{MgSiO}_3$  phase relations: Cen = clinoenstatite, Maj = majorite, Ilm = ilmenite, and Pv = perovskite.  $\beta$  represents  $\beta\text{-Mg}_2\text{SiO}_4$ ;  $\gamma$  =  $\gamma\text{-Mg}_2\text{SiO}_4$ ; and St = stishovite, phase boundaries with these phases were not calculated in this study. The dashed lines represent the results if the pressure effects on the entropy change  $\Delta S$  for the transition are not included, and the solid lines represent the results if the pressure effects on  $\Delta S$  are included in Equation 1. Table 9 lists the slopes of each of the transitions estimated here.

lower than previous calorimetry. The mode Grüneisen parameters listed in the density of states model (Table 2) reflect those of the high-pressure measurements.

### PEROVSKITE

Details of the thermodynamic properties from vibrational spectroscopy at ambient conditions and high pressures have already been published (Chopelas 1996; Chopelas et al. 1994a). For completeness: In  $Pbnm$   $\text{MgSiO}_3$  perovskite, there are four formula units per unit cell giving a total of 60 vibrations at any one point in the Brillouin zone. At the Brillouin zone center, these modes are distributed among the following symmetry species:  $7A_g(\text{R}) + 7B_g(\text{R}) + 5B_{2g}(\text{R}) + 5B_{2g}(\text{R}) + 8A_u + 8B_{1u}(\text{IR}) + 10B_{2u}(\text{IR}) + 10B_{3u}(\text{IR})$ . Thus, there are three acoustic modes ( $B_{1u}$ ,  $B_{2u}$ , and  $B_{3u}$  symmetry), 24 Raman modes, and 25 infrared modes. Recent infrared data (Lu et al. 1994) provided peak positions for the expected 25 infrared modes. The Raman data for  $\text{MgSiO}_3$  perovskite is incomplete where only 11 modes have been identified (Durben and Wolf 1992). However, recent polarized single-crystal spectra of  $\text{GdAlO}_3$  and  $\text{YAlO}_3$  (Chopelas et al. 1994b) revealed 22 of the 24 expected Raman modes, thus providing valuable clues for the distribution of the modes in  $\text{MgSiO}_3$  perovskite. The final density of states, Table 2 bottom, based on the above information, yields heat capacity  $C_p$  values in good agreement with recent calorimetric measurements (Akaogi and Ito 1993a) as

**TABLE 8.** Heat capacities at 300 and 1000 K for  $\text{MgO-SiO}_2$  phases

Phase	300 K	1000 K	Phase	300 K	1000 K
Forsterite	119.0	174.6	Oen	81.7	127.5
$\beta$	114.1	173.1	Cen	80.4	125.2
$\gamma$	113.2	172.5	Maj	80.5	122.7
Pv + MgO	120.2	181.5	Ilm	78.0	123.1
			Pv	82.8	123.9

Note: Calculated using Equations 2 and 3 with the vibrational models in Table 2 and from previous work (Chopelas 1990, 1991; Chopelas et al. 1994a).

previously reported (Chopelas et al. 1994a, Chopelas 1996).

High-pressure spectra of perovskite (1) yield information on how the density of states changes with pressure, and (2) reveal that there is a profound change in compression mechanism at about 40 GPa. This has been confirmed by recent measurements on perovskite to 100 GPa (Serghiou et al. 1998). For the thermodynamic calculations on perovskite, the pressure shifts of the modes below 40 GPa were used.

All of the  $\text{MgSiO}_3$  polymorphs investigated in this study, except ilmenite, exhibit some sort of non-quenchable phase change. For ilmenite, the experimental pressures did not exceed the stability pressures for this material and thus were too low to provide a driving force. However, for all other phases, the dominant peaks in the spectrum disappear or new dominant peaks appear and the pressure dependencies of most modes change quite dramatically, decreasing often to less than half their previous values. This type of behavior appears to be the rule rather than the exception for  $\text{MgSiO}_3$  phases.

### PHASE DIAGRAM CALCULATIONS

In addition to the data on the  $\text{MgSiO}_3$  polymorphs, thermodynamic data on  $\beta\text{-Mg}_2\text{SiO}_4$ ,  $\gamma\text{-Mg}_2\text{SiO}_4$ , and stishovite are needed to complete the phase diagram for  $\text{MgSiO}_3$ . The  $\beta$  to  $\gamma$  phase transition already has been calculated using the methods in this report (Chopelas et al. 1994a) and the phase boundaries with stishovite are not included here.

Tables 6 and 7 lists the enthalpies, thermal expansivities, bulk moduli and their pressure dependencies, and the molar volumes at room conditions, which are needed to complete these calculations using Equations 1 to 4. A first attempt was made to constrain the phase diagram without the phase equilibrium data, but in most cases the uncertainties of the enthalpies were too high and the phase boundaries were not at all consistent with observations. In these cases, points were chosen on the phase boundaries and the enthalpies were estimated using the previous volume and present entropy estimates. In all cases, the resulting enthalpies were well within the uncertainty limits given in calorimetric results (listed in Yusa et al. 1993). For the unquenchable clinopyroxene phase, this was the only way to obtain a phase boundary using Equations

tion 1. The new results are shown in Figure 10. Garnet disorder was not taken into consideration in the calculations because the disorder appears to be very small in MgSiO<sub>3</sub> garnet as observed by two different measurements (Angel et al. 1989; Phillips et al. 1992). Slopes for the various phase changes in this diagram are listed in Table 8. The present results show linear Clapeyron slopes, whereas the previous results show pronounced curvature over the large *P-T* range in their diagram (Yusa et al. 1993). Sources for this fundamental difference were sought and the following were noted. In the previous work, values of  $\Delta V$  were altered for different *P-T* conditions, whereas values of  $\Delta H$  and  $\Delta S$  were not. Upon closer examination of the interrelationships among these thermodynamic parameters, the phase boundary curvature in the previous calculations can be understood.

Changes in  $\Delta H$  due to temperature (and pressure) variations can be evaluated using the heat capacity in Equation 5. Looking at the heat capacities of several polymorphs in this system (Table 8), at two different temperatures the heat capacities between phases with the same chemical formula do not vary by much. This means that the change in enthalpy across phase transitions varies by an amount smaller than the stated uncertainties for  $\Delta H$  at any given point in *P-T* space. Therefore, assuming a constant enthalpy, change for all *P-T* space will not affect the results significantly.

Changes in  $\Delta S$  for the transitions due to temperature and pressure variations can be evaluated by using the vibrational models. This has been done for several materials (Chopelas 1990, 1991, 1996; Chopelas et al. 1994a). An interdependence between entropy and volume in a given phase at different *P-T* conditions can be seen by considering the equation for the entropy of a gas:

$$\Delta S = nR \ln \frac{V_2}{V_1} \quad (6)$$

where *n* is the number of moles and *R* is the universal gas constant. Although the materials here are solids, this simple relationship shows that entropy and volume are not independent variables. The changes in  $\Delta S$  are quite small (on the order of a few percent) but are large enough to change the topography of a phase diagram calculation over long extrapolations. Close examination of the relationship between *S* and *V* for the forsterite to  $\beta$ -phase transition (Chopelas 1991) showed that  $\Delta S/\Delta V$  changed by an amount much smaller than the experimental error over a large temperature and pressure range. A further illustration is shown in Table 8, which lists the slopes of the various transitions examined in this study while either keeping  $\Delta S$  constant or while varying it as a function of pressure for use in Equation 1. The Clapeyron slopes are overestimated by 20 to 100% if  $\Delta S$  is held constant. Neglecting the changes in  $\Delta S$  will also lead to exaggerated curvature in the phase boundaries. It is clear that if one alters  $\Delta V$  for pressure and temperature in Equation 1, one must also alter  $\Delta S$ .

**TABLE 9.** Slopes resulting from taking  $\Delta S$  as a constant or  $\Delta S$  as a function of pressure

Transition	Slope (bar/K)	
	Constant $\Delta S$	$\Delta S(P)$
Oen-Cen	50	31
Cen-Maj	-5.4	-12
Maj-Ilm	68	46
Ilm-Pv	-36	-46
Maj-Pv	46	26

## ACKNOWLEDGMENTS

Thanks go to the two reviewers of this paper, Pamela Conrad and one anonymous, and George Serghiou for helpful comments, which improved this paper.

## REFERENCES CITED

- Akaogi, M. and Ito, E. (1993a) Heat capacity of MgSiO<sub>3</sub> perovskite. *Geophysical Research Letters*, 20, 105–108.
- (1993b) Refinement of enthalpy measurement of MgSiO<sub>3</sub> perovskite and negative pressure-temperature slopes for perovskite-forming reactions. *Geophysical Research Letters*, 20, 1839–1842.
- Akaogi, M., Ito, E., and Navrotsky, A. (1989) Olivine- modified spinel-spinel transitions in the system Mg<sub>2</sub>SiO<sub>4</sub>-Fe<sub>2</sub>SiO<sub>4</sub>: Calorimetric measurements, thermochemical calculation, and geophysical application. *Journal of Geophysical Research*, 94, 15671–15685.
- Akaogi, M., Ross, N.L., McMillan, P., and Navrotsky, A. (1984) The Mg<sub>2</sub>SiO<sub>4</sub> polymorphs (olivine, modified spinel, and spinel): thermodynamic properties for oxide solution calorimetry, phase relations, and models of lattice vibrations. *The American Mineralogist*, 29, 499–512.
- Angel, R.J., Chopelas, A., and Ross, N.L. (1992) Stability of high-density clinenstatite at upper-mantle pressures. *Nature*, 358, 322–324.
- Angel, R.J., Finger, L.W., Hazen, R.M., Kanzaki, M., Weidner, D.J., Liebermann, R.C., and Veblen, D.R. (1989) Structure and twinning of single-crystal MgSiO<sub>3</sub> garnet synthesized at 17 GPa and 1800 °C. *American Mineralogist*, 74, 509–512.
- Ashida, T., Kume, E., Ito, E., and Navrotsky, A. (1988) MgSiO<sub>3</sub> ilmenite: heat capacity, thermal expansivity, and enthalpy of transformation. *Physics and Chemistry of Minerals*, 16, 239–245.
- Birch, F. (1978) Finite strain isotherm and velocities for single crystal and polycrystalline NaCl at high pressures and 300 K. *Journal of Geophysical Research*, 83, 1257–1268.
- Boehler, R. and Chopelas, A. (1992) Phase transitions in a 500 kbar – 3000 K gas apparatus. In Y. Syono and M.H. Manghnani, Eds. *High-Pressure Research: Application to Earth and Planetary Sciences*, p. 55–60. Terrapub, Tokyo.
- Chopelas, A. (1990) Thermal expansion, heat capacity, and entropy of MgO at mantle pressures. *Physics and Chemistry of Minerals*, 17, 142–148.
- (1991) Thermal properties of  $\beta$ -Mg<sub>2</sub>SiO<sub>4</sub> at mantle pressures derived from vibrational spectroscopy: Implications for the mantle at 400 km depth. *Journal of Geophysical Research*, 96, 11817–11829.
- (1996) Thermal expansivity of lower mantle phases MgO and MgSiO<sub>3</sub> perovskite at high pressure derived from vibrational spectroscopy. *Physics of the Earth and Planetary Interiors*, 98, 3–15.
- Chopelas, A. and Boehler, R. (1992a) Raman spectroscopy of high-pressure MgSiO<sub>3</sub> phases synthesized in a CO<sub>2</sub> laser heated diamond-anvil cell. In Y. Syono and M. Manghnani, Eds. *High Pressure Research: Application to Earth and Planetary Science*, p. 101–108. Terrapub, Tokyo.
- (1992b) Thermal expansivity in the lower mantle. *Geophysical Research Letters*, 19, 1983–1986.
- Chopelas, A., Boehler, R., and Ko, J. (1994a) Thermodynamics and Behavior of  $\gamma$ -Mg<sub>2</sub>SiO<sub>4</sub> at high pressure: implications for Mg<sub>2</sub>SiO<sub>4</sub> phase equilibrium. *Physics and Chemistry of Minerals*, 21, 351–359.
- Chopelas, A., Reichmann, H.J., and Hofmeister, A.M. (1994b) Is the extrapolation of physical properties of orthorhombic MgSiO<sub>3</sub> perovskite to lower mantle conditions valid? (abstract). *EoS Transactions of the American Geophysical Union*, 75, 596.

- Durben, D.J. and Wolf, G.H. (1992) High-temperature behavior of metastable  $\text{MgSiO}_3$  perovskite: a Raman spectroscopic study. *American Mineralogist*, 77, 890–893.
- Etchepare, J. (1970) Study by Raman spectroscopy of crystalline and glassy diopside. *Amorphous materials, Third International Conference*, p. 337–346.
- Fateley, W.G., McDevitt, N.T., and Bently, F.F. (1971) Infrared and Raman selection rules for lattice vibrations: the correlation method. *Applied Spectroscopy*, 25, 155–174.
- Flesch, L.M., Li, B., and Liebermann, R.C. (1998) Sound velocities of polycrystalline  $\text{MgSiO}_3$ -orthopyroxene to 10 GPa at room temperature. *American Mineralogist*, 83, 444–451.
- Hofmeister, A.M. and Chopelas, A. (1991a) Thermodynamic properties of pyrope and grossular from vibrational spectroscopy. *The American Mineralogist*, 76, 880–891.
- (1991b) Vibrational spectroscopy of end-member silicate garnets. *Physics and Chemistry of Minerals*, 17, 503–526.
- Hofmeister, A.M. and Ito, E. (1992) Thermodynamic properties of  $\text{MgSiO}_3$  ilmenite from vibrational spectra. *Physics and Chemistry of Minerals*, 18, 423–432.
- Hugh-Jones, D.A. and Angel, R.J. (1994) A compressional study of  $\text{MgSiO}_3$  orthoenstatite up to 8.5 GPa. *American Mineralogist*, 79, 405–410.
- Krupka, K.M., Hemingway, B.S., Robie, R.A., and Kerrick, D.M. (1985a) High-temperature heat capacities and derived thermodynamic properties of anthophyllite, diopside, dolomite, enstatite, bronzite, talc, tremolite, and wollastonite. *American Mineralogist*, 70, 261–271.
- Krupka, K.M., Robie, R.A., Hemingway, B.S., Kerrick, D.M., and Ito, J. (1985b) Low-temperature heat capacities and derived thermodynamic properties of anthophyllite, diopside, enstatite, bronzite, and wollastonite. *American Mineralogist*, 70, 249–260.
- Lu, R., Hofmeister, A.M., and Wang, Y. (1994) Thermodynamic properties of ferromagnesian silicate perovskites from vibrational spectroscopy. *Journal of Geophysical Research*, 99, 11795–11804.
- McMillan, P., Akaogi, M., Ohtani, E., Williams, Q., Nieman, R., and Sato, R. (1989) Cation disorder in garnets along the  $\text{Mg}_3\text{Al}_2\text{Si}_3\text{O}_{12}$ - $\text{Mg}_4\text{Si}_4\text{O}_{12}$  join: an infrared, Raman and NMR study. *Physics and Chemistry of Minerals*, 16, 428–435.
- Pacalo, R.E.G. and Gasparik, T. (1990) Reversals of the orthoenstatite-clinoenstatite transition at high pressures and high temperatures. *Journal of Geophysical Research*, 95, 15853–15858.
- Phillips, B.L., Howell, D.A., Kirkpatrick, R.J., and Gasparik, T. (1992) Investigation of cation order in  $\text{MgSiO}_3$  garnet using  $^{29}\text{Si}$  and  $^{27}\text{Al}$  MAS NMR spectroscopy. *American Mineralogist*, 77, 704–712.
- Rauch, M., Keppler, H., and Wokaun, A. (1996) A pressure-induced phase transition in  $\text{MgSiO}_3$ -rich garnet revealed by Raman spectroscopy. *American Mineralogist*, 81, 1289–1292.
- Reynard, B. and Rubie, D.C. (1996) High-pressure high-temperature Raman spectroscopic study of  $\text{MgSiO}_3$  ilmenite. *American Mineralogist*, 81, 1092–1096.
- Serghiou, G., Zerr, A., and Boehler, R. (1998)  $(\text{Mg,Fe})\text{SiO}_3$ -stability under lower mantle conditions. *Science*, 280, 2093–2095.
- Weidner, D.J. and Ito, E. (1985) Elasticity of  $\text{MgSiO}_3$  in the ilmenite phase. *Physics of the Earth and Planetary Interiors*, 40, 65–70.
- Weidner, D.J., Wang, Y., and Yeganeh-Haeri, A. (1993) Equation of state properties of mantle perovskites (abstract). *EOS Transactions of the American Geophysical Union*, 74, 571.
- Yagi, T., Uchiyama, Y., Akaogi, M., and Ito, E. (1992) Isothermal compression curve of  $\text{MgSiO}_3$  tetragonal garnet. *Physics of the Earth and Planetary Interiors*, 74, 1–7.
- Yusa, H., Akaogi, M., and Ito, E. (1993) Calorimetric study of  $\text{MgSiO}_3$  garnet and pyroxene: Heat capacities, transition enthalpies, and equilibrium phase relations in  $\text{MgSiO}_3$  at high pressures and temperatures. *Journal of Geophysical Research*, 98, 6453–6460.

MANUSCRIPT RECEIVED MAY 19, 1998

MANUSCRIPT ACCEPTED SEPTEMBER 16, 1998

PAPER HANDLED BY ROBERT M. HAZEN